Full Utilization of Superior Charge-Discharge Characteristics of $Na_{1.56}Fe_{1.22}P_2O_7$ Positive Electrode by Using Ionic Liquid Electrolyte

Chih-Yao Chen, Kazuhiko Matsumoto,* Toshiyuki Nohira,*,z and Rika Hagiwara*,z

Graduate School of Energy Science, Kyoto University, Sakyo-ku, Kyoto 606–8501, Japan

$Na_{1.56}Fe_{1.22}P_2O_7$ was synthesized via a conventional solid-state method and evaluated as a positive electrode for Na secondary batteries using Na[FSA]–[C_3C_1pyrr][FSA] (C_3C_1pyrr = *N*-methyl-*N*-propylpyrrolidinium and FSA = bis(fluorosulfonyl)amide) ionic liquids (IL) as electrolytes, over the temperature range of 298–363 K. A reversible capacity as high as 108 mAh g^{-1} has been achieved for the first time with a thermally stable IL at 363 K. This value is close to the theoretically calculated capacity of 118 mAh g^{-1} and is significantly higher than the previously reported values of *ca.* 85 mAh g^{-1} in organic electrolytes at 298 K. The capacity of 108 mAh g^{-1} also exceeds the value obtained for $Na_2FeP_2O_7$ electrodes (94 mAh g^{-1}) under the same experimental conditions. Moreover, excellent rate capability and superior cyclability exceeding 3000 cycles have been achieved by using the IL electrolyte over a wide temperature range of 298–363 K.

 [DOI: 10.1149/2.0931501jes]

Manuscript submitted September 16, 2014; revised manuscript received October 27, 2014. Published November 25, 2014.

Recently, it has been recognized that Na secondary batteries can offer a performance comparable to that of Li batteries, at a more reasonable cost.[1,2] Developing commercial Na secondary batteries that are economically viable, safe, and have a long life will definitely require the development of new electrode materials and electrolytes.[3] Layered oxides in the form of Na_xMO_2 (where M is a transition metal) have been extensively tested as Na host materials,[4–8] and some of the oxides have exhibited considerably high Na storage capacities by suitably tailoring the stoichiometric ratio of Na to M.[6–8] However, most of these materials undergo complicated phase transitions during cycling[4–6] and may result in limited cyclability,[5–7] which is an obstacle for practical applications.[8]

In order to overcome such limitations in electrode performance, phosphate-based framework materials have been proposed as positive electrode materials in Na secondary batteries.[9–16] The robust framework undergoes a topotactic Na insertion/extraction reaction with a small volume change upon electrochemical cycling. Among them, pyrophosphates ($Na_2MP_2O_7$, where M = Fe, Mn, or Co) have attracted interest owing to their favorable electrochemical activity and good thermal stability.[10–16] However, they are less appealing in terms of theoretical capacity (*ca.* 97 mAh g^{-1}, 1 Na per formula unit) as compared to layered oxides (*ca.* 120 mAh g^{-1}, 0.5 Na per formula unit), owing to the presence of the P_2O_7 units that induce a weight penalty.

Recently, $Na_{2-x}Fe_{1+x/2}P_2O_7$ compounds (where, $0 < x < 0.44$) were synthesized and evaluated as positive electrodes for Na secondary batteries using organic electrolytes at room temperature.[17,18] The substitution of Na with Fe would directly influence the active Na sites and the coordination environment of the redox center, resulting in distinct electrochemical characteristics. Notably, the theoretical capacity for the extreme stoichiometric composition, $Na_{1.56}Fe_{1.22}P_2O_7$ ($x = 0.44$), is estimated to be increased to the highest value of 118 mAh g^{-1}, assuming that 1.22 Na is reversibly intercalated/deintercalated via the redox reaction of 1.22 Fe^{2+}/Fe^{3+}. A comparison between the end members of $Na_{2-x}Fe_{1+x/2}P_2O_7$ (i.e., $x = 0$ and 0.44) is therefore of importance, as it would provide an avenue for the electrochemical properties of the pyrophosphates to be maximized through composition design. However, the full theoretical capacity of $Na_{1.56}Fe_{1.22}P_2O_7$ has not been realized so far. The capacity values typically reported in the literature are *ca.* 85 mAh g^{-1} and generally include only results of limited cycles.[17,18]

Ionic liquids (ILs) have been proposed as replacements for conventional electrolytes because of its advantages such as nonflammability, good thermal and electrochemical stability compared to organic solvents.[19,20] Recent advances in the field of Li secondary batteries have suggested that ILs represent a viable alternative to overcome the disappointing compromises between performance and safety features with organic electrolytes.[20,21] However, the adoption of IL electrolytes for Na batteries has received less attention so far.[22,23]

In our previous studies, the charge–discharge behavior of $Na_2FeP_2O_7$ electrodes in Na[FSA]–[C_3C_1pyrr][FSA] (where FSA = bis(fluorosulfonyl)amide and C_3C_1pyrr = *N*-methyl-*N*-propylpyrrolidinium) IL electrolytes was investigated over a wide temperature range of 253–363 K.[24] The results revealed a considerable enhancement in rate capability with increasing temperature along with an outstanding cyclability, implying that there are significant opportunities to improve the performance of Na secondary batteries by utilizing an IL electrolyte. Another advantage of using IL electrolytes is that the operation of the batteries at high temperatures is favorable to fully draw the potential capacity of the electrode material.

In the present work, the electrochemical properties of $Na_{1.56}Fe_{1.22}P_2O_7$ in the Na[FSA]–[C_3C_1pyrr][FSA] IL electrolyte system at 298–363 K are investigated and compared to those of $Na_2FeP_2O_7$ under the same conditions, in order to understand the effect of altering the stoichiometric ratio of Na to Fe, in a polyanion-type positive electrode. The dependence of the rate capability and the cyclability of these electrodes on temperature are also examined.

Experimental

$Na_{2-x}Fe_{1+x/2}P_2O_7$ with extreme compositions, (namely, $x = 0$ and 0.44) were synthesized using a solid-state method.[25] Stoichiometric amounts of Na_2CO_3, $FeC_2O_4 \cdot 2H_2O$ and $(NH_4)_2HPO_4$ were mixed thoroughly by ballmilling for 8 h. The mixture was initially heated at 573 K for 6 h and then heated at 873 K for 12 h under Ar flow. X-ray diffraction (XRD) data were collected using a Rigaku SmartLab diffractometer equipped with a one-dimensional high-speed Si strip detector (D/teX Ultra), utilizing Cu Kα radiation (40 kV and 30 mA). The structural refinement was carried out by the Rietveld method in an iterative procedure using the RIETAN-FP software package.[26] The obtained structure was evaluated based on R_{wp} and R_p defined as follows:

$$R_{wp} = \left\{ \frac{\sum_i w_i [y_{C,i} - y_{O,i}]^2}{\sum_i w_i [y_{O,i}]^2} \right\}^{1/2} \qquad R_p = \frac{\sum_i |y_{C,i} - y_{O,i}|}{\sum_i y_{O,i}}$$

*Electrochemical Society Active Member.
zE-mail: nohira@energy.kyoto-u.ac.jp; hagiwara@energy.kyoto-u.ac.jp

$y_{C,i}$ and $y_{O,i}$ are intensity values of diffraction data, where C and O indicate computed and observed values. The weight is labeled as w_i. The crystal structures were visualized using the VESTA software.[27] The morphology of the sample was observed using field-emission scanning electron microscopy (FE-SEM, Hitachi SU-8020). The composition of the sample was analyzed for Na, and Fe and P using atomic absorption spectrometry (AAS, Hitachi Z2300) and inductively coupled plasma atomic emission spectroscopy (ICP-AES, SII SPS4000), respectively.

The electrochemical properties of $Na_{2-x}Fe_{1+x/2}P_2O_7$ were assessed using 2032 type coin cells with a Bio-Logic VSP potentiostat.[24,28] The positive electrode was prepared by mixing $Na_{2-x}Fe_{1+x/2}P_2O_7$, acetylene black and polytetrafluoroethylene in a weight ratio of 75:20:5. The mass loading and thickness of the active material were around 2.0 mg cm^{-2} and 50 μm, respectively. A metallic sodium disc pressed onto an aluminum current collector was used as the negative electrode. A Na[FSA]–[C_3C_1pyrr][FSA] (in a 20:80 molar ratio) ionic liquid was utilized as the electrolyte. Na[FSA] and [C_3C_1pyrr][FSA] were dried under vacuum for 24 h at 353 K and 333 K, respectively. The separator was impregnated under vacuum with the electrolyte at 333 K for 48 h prior to the test. The theoretical capacity of $Na_2FeP_2O_7$ and $Na_{1.56}Fe_{1.22}P_2O_7$ were defined as 97 mAh g^{-1} and 118 mAh g^{-1}, respectively, corresponding to a one-electron transfer per redox-active metal.

Results and Discussion

Although $Na_{1.56}Fe_{1.22}P_2O_7$ was first synthesized and characterized using single crystal X-ray diffraction by Angenault et al. in 1995, no electrochemical data was reported in that work.[29] The XRD pattern and the Rietveld refinement results of the as-synthesized $Na_{1.56}Fe_{1.22}P_2O_7$ are shown in Fig. 1. No obvious diffraction peaks from impurities are detected. The $Na_{1.56}Fe_{1.22}P_2O_7$ sample crystallizes into the space group *P*-1, with $a = 6.4215(3)$ Å, $b = 9.390(4)$ Å, $c = 10.978(4)$ Å, $\alpha = 64.546(10)^\circ$, $\beta = 86.091(12)^\circ$, $\gamma = 73.013(13)^\circ$, $V = 569.8(4)$ Å^3, and $Z = 4$. The lattice parameters of $Na_{1.56}Fe_{1.22}P_2O_7$ are in good agreement with previously reported microcrystalline and single crystal data.[18,29] Unit cell parameters are presented in Table S1 (Supplementary material).

A compositional analysis of the as-synthesized $Na_{1.56}Fe_{1.22}P_2O_7$ was conducted using ICP-AES and AAS. The atomic ratio of Na/Fe/P is determined to be 1.47:1.22:2. The consistency between the analytical result obtained above and the expected compound verifies the feasibility of solid-state method adopted. $Na_{1.56}Fe_{1.22}P_2O_7$ exhibits a broad size distribution ranging from hundreds of nanometers to a few micrometers (Fig. 1, inset) and no distinct differences in the morphology are found when compared with $Na_2FeP_2O_7$. The Rietveld refinement results for $Na_2FeP_2O_7$, synthesized by the same solid-state method have been reported in our previous study.[24]

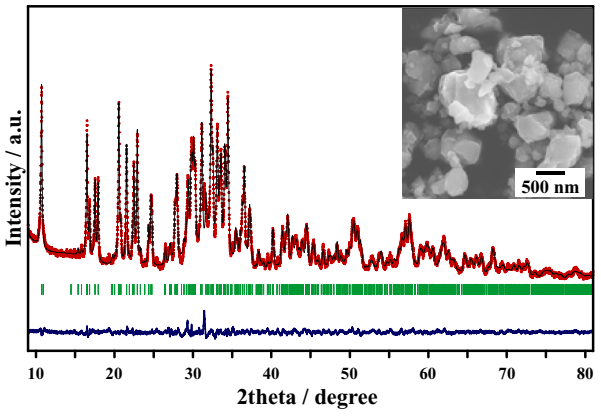

Figure 1. X-ray diffraction pattern with the Rietveld refinement results of $Na_{1.56}Fe_{1.22}P_2O_7$ (R_{wp} = 0.88% and R_p = 0.60%); experimental data (red dots), calculated pattern (black line), Bragg positions (green bars) and the difference curve (blue line). (Inset) SEM image of the as-synthesized $Na_{1.56}Fe_{1.22}P_2O_7$.

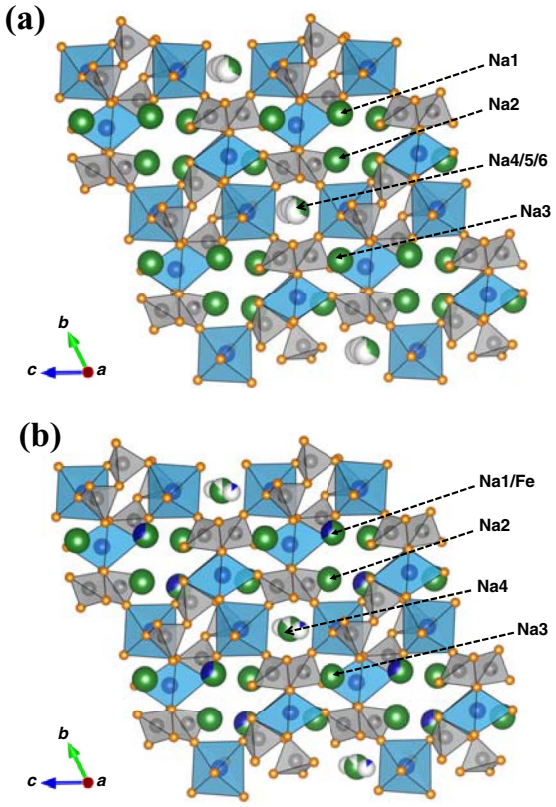

Figure 2. Crystal structures of (a) $Na_2FeP_2O_7$ and (b) $Na_{1.56}Fe_{1.22}P_2O_7$, with FeO_6 and PO_4 polyhedra shown in blue and gray, respectively. Na, Fe, P and O are green, blue, gray and orange, with the shading indicating occupancy.

A comparative study of the crystal structures of $Na_{1.56}Fe_{1.22}P_2O_7$ and $Na_2FeP_2O_7$ reveals the similarities and the differences between them. According to the structural models proposed for $Na_{1.56}Fe_{1.22}P_2O_7$ and $Na_2FeP_2O_7$,[11,29] both the compounds possess a similar framework in which the FeO_6 octahedra interconnect with the P_2O_7 units resulting in three-dimensional and large interstitial spaces through which Na ions can diffuse (Fig. 2). On the other hand, compared to $Na_2FeP_2O_7$, the occupancy of Na6 sites is reduced to 0 and the occupancy of Na4 sites is increased from 0.333 to 0.882 in the case of $Na_{1.56}Fe_{1.22}P_2O_7$. The Na5 sites are partially occupied by Fe with an occupancy of 0.118 in addition to one Na site in the large tunnel along the *a* axis (Na1) being partly replaced by Fe in $Na_{1.56}Fe_{1.22}P_2O_7$, whereas no site mixing is found in $Na_2FeP_2O_7$. The presence of co-occupied sites results in a much larger mean value for the cation–oxygen bond length compared to that of the other FeO_6 units ($r_{Na}{}^{+}$ = 1.02 Å > $r_{Fe}{}^{2+}$ = 0.78 Å).[29] Therefore, polyhedral units are considered to be more distorted in $Na_{1.56}Fe_{1.22}P_2O_7$ than in $Na_2FeP_2O_7$.

The galvanostatic charge–discharge curves of the $Na_{1.56}Fe_{1.22}P_2O_7$ and $Na_2FeP_2O_7$ electrodes at a current density of 10 mA g^{-1} at 298 and 363 K are compared in Fig. 3. $Na_2FeP_2O_7$ delivers reversible capacities of 90 mAh g^{-1} and 94 mAh g^{-1} in the voltage range of 2.0–4.0 V at 298 K and 363 K, respectively. In addition, an apparent shift in the plateau potential from the first charging to the subsequent charging cycles is observed at both temperatures. This phenomenon has been ascribed to a Na deficiency in the pristine state caused by oxidative contamination on the particle surface upon ambient exposure.[12,30,31] In comparison with $Na_2FeP_2O_7$, $Na_{1.56}Fe_{1.22}P_2O_7$ clearly shows better electrochemical characteristics under the same

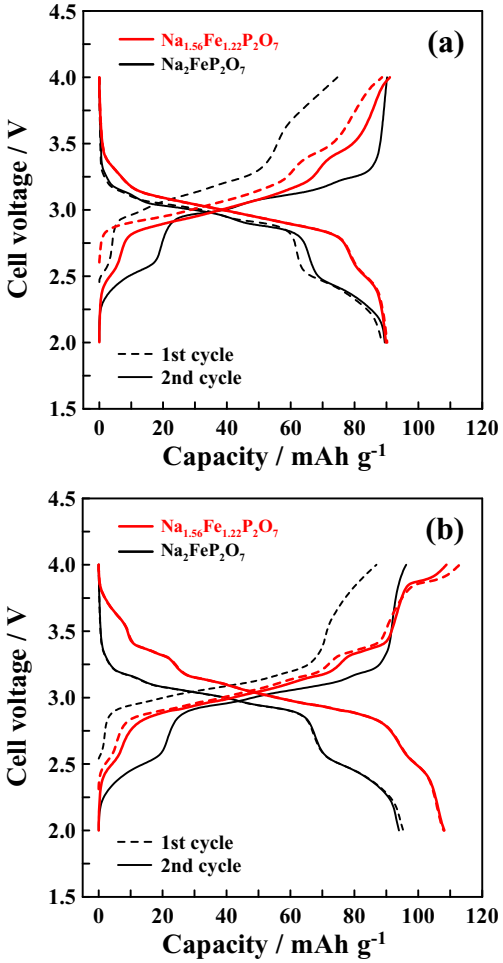

Figure 3. Galvanostatic charge–discharge curves for the Na/Na[FSA]–[C_3C_1pyrr][FSA]/$Na_{2-x}Fe_{1+x/2}P_2O_7$ (x = 0 and 0.44) cells at a current density of 10 mA g^{-1} in the voltage range 2.0–4.0 V at (a) 298 K and (b) 363 K. $Na_{1.56}Fe_{1.22}P_2O_7$: Red line. $Na_2FeP_2O_7$: black line.

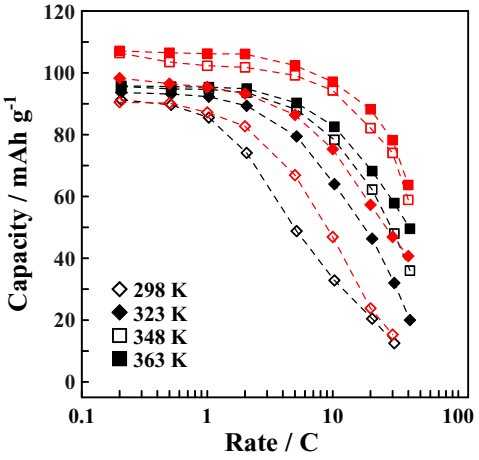

Figure 4. The rate capability of the $Na_{2-x}Fe_{1+x/2}P_2O_7$ (x = 0 and 0.44) positive electrodes over the 298–363 K temperature range. The cell was charged at C/10. Cut-off voltage: 2.0–4.0 V. $Na_{1.56}Fe_{1.22}P_2O_7$: Red line. $Na_2FeP_2O_7$: black line.

experimental conditions. At 298 K, the $Na_{1.56}Fe_{1.22}P_2O_7$ electrode exhibits a smooth charge–discharge profile, a smaller voltage shift during the first charging cycle, and a reversible capacity of 90 mAh g^{-1}. At 363 K, the voltage shift for the $Na_{1.56}Fe_{1.22}P_2O_7$ electrode becomes almost negligible and the reversible capacity is evidently improved by 15% (108 mAh g^{-1}), which corresponds to approximately 92% of the theoretical capacity based on the one-electron reaction. The well-overlapped feature of the first and the second charging curves implies that $Na_{1.56}Fe_{1.22}P_2O_7$ may be more resistant to atmospheric poisoning, resulting in better preservation of the initial stoichiometry.

Notably, the voltage profiles of $Na_{1.56}Fe_{1.22}P_2O_7$ and $Na_2FeP_2O_7$ also exhibit a pronounced difference at 363 K. While two distinguishable voltage plateaus are observed at 2.5 V and 3.0 V in the case of $Na_2FeP_2O_7$, for $Na_{1.56}Fe_{1.22}P_2O_7$ the plateau at 2.5 V becomes narrower while a new plateau appears at 3.8 V (Fig. 3b). For $Na_2FeP_2O_7$, it was reported that the presence of several distinct crystallographic Na sites and their ordering lead to multistep voltage-capacity profiles.[11] Since the distributions of constituent Na atoms and their ordering are different between $Na_{1.56}Fe_{1.22}P_2O_7$ and $Na_2FeP_2O_7$, the voltage profiles are altered. Besides, the distinct voltage profiles imply that the active Na intercalation/deintercalation sites of the two compounds are altered as the ratio of Na to Fe is varied. The results also indicate that the operating voltage is influenced by the local environment of the polyanions.[32] An upward shift in the discharge curves is observed for $Na_{1.56}Fe_{1.22}P_2O_7$, leading to a higher average operating voltage.

Honma et al. has reported that while $Na_{2-x}Fe_{1+x/2}P_2O_7$/C composites with different stoichiometries (i.e., x values of 0, 0.22, and 0.44) can be synthesized by glass-ceramic routes, their reversible discharge capacities remain constant at *ca.* 86 mAh g^{-1} in $NaPF_6$/EC:DEC electrolytes at 298 K.[17] Ha et al. has performed an off-stoichiometric synthesis with a nominal composition of $Na_{3.42}Fe_{2.44}(P_2O_7)_{2.05}$. They concluded that the sample was comprised of a Na-rich $Na_{1.66}Fe_{1.17}P_2O_7$ phase and an inactive $NaFePO_4$ phase.[18] For the composites, a reversible capacity of about 85 mAh g^{-1} was obtained in $NaClO_4$/EC:DEC at C/20 at 303 K. The room temperature capacity (*ca.* 90 mAh g^{-1}) obtained in the present IL electrolyte is slightly higher than those obtained in the organic electrolytes under similar conditions, which could be explained by the successful synthesis of $Na_{1.56}Fe_{1.22}P_2O_7$. More importantly, the present result confirms that a moderately elevated operating temperature can effectively enhance the utilization ratio of the active materials, resulting in a higher capacity.

Fig. S1 (Supplementary material) shows ex-situ XRD patterns of as-synthesized, fully charged and fully discharged $Na_{1.56}Fe_{1.22}P_2O_7$. For the fully charged sample, there are several splits and shifts of diffraction peaks when compared with the as-synthesized $Na_{1.56}Fe_{1.22}P_2O_7$. However, the overall framework of crystal structure seems to be preserved. For the fully discharged sample, the diffraction pattern coincides with that for as-synthesized $Na_{1.56}Fe_{1.22}P_2O_7$, confirming that the reaction is reversible. The diffraction pattern of charged sample is in agreement with the previous report by Ha et al. in which they prepared a series of $Na_{1.56-x}Fe_{1.22}P_2O_7$ via chemical sodiation and desodiation.[18] They concluded that there were no apparent evidences for the formation of a new phase in the fully charged state, indicating that the $Na_{1.56}Fe_{1.22}P_2O_7$ electrode undergoes a single-phase reaction.[18]

The rate capability of the $Na_{1.56}Fe_{1.22}P_2O_7$ electrode was evaluated over a temperature range of 298–363 K. The cells were charged to 4.0 V at a constant current density of C/10 (11.8 mA g^{-1}), and subsequently discharged to 2.0 V at various rates. The discharge capacity of the $Na_{2-x}Fe_{1+x/2}P_2O_7$ electrode plotted as a function of the discharge rates and temperatures is shown in Fig. 4. The capacities decrease with increasing current densities for all the cells because the reactions are kinetically constrained at high rates. Nevertheless, the capacities remain at 77%, 89%, and 90% for the cells tested at 323, 348, and 363 K, respectively when the discharge rate is increased from C/5 to 10 C. The reversible capacities at 363 K are 106, 97, 88, 78, and 64 mAh g^{-1} at discharge rates of 2 C, 10 C, 20 C, 30 C, and 40 C, respectively. It may be noted that carbon coating and/or nanosizing are not necessary to obtain such electrode performance. Clark et al.

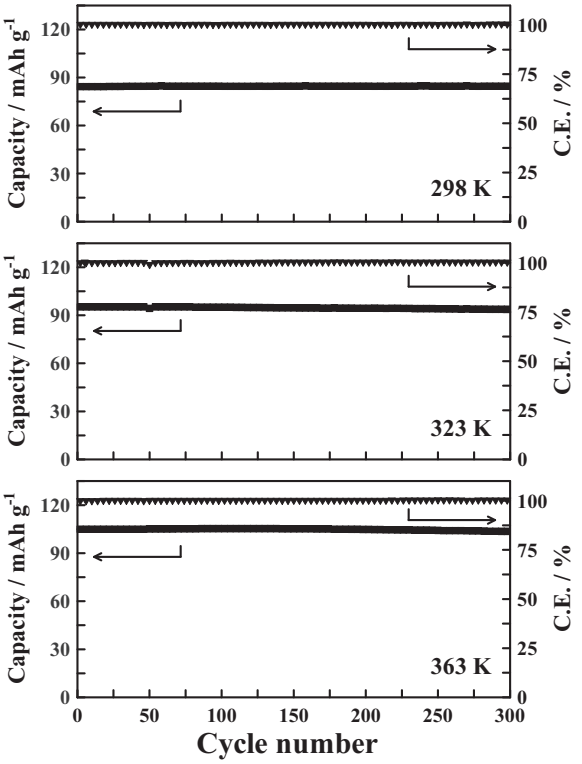

Figure 5. Cycling performance and coulombic efficiency (C.E.) of the $Na_{1.56}Fe_{1.22}P_2O_7$ positive electrode at 298, 323, and 363 K. Cut-off voltage: 2.0–4.0 V; current density: 1 C (118 mA g^{-1}).

have studied the diffusion behavior of Na in $Na_2FeP_2O_7$ by atomistic simulation methods.[33] Their results revealed that $Na_2FeP_2O_7$ provides quasi-three-dimensional (3D) Na ion diffusion paths with acceptably low activation energies in all crystallographic directions. Ion blocking by Na/Fe antisite defects is therefore much less likely to impede its transport properties when compared to other materials such as $NaFePO_4$ and Na_2FePO_4F in which only 1D and 2D conduction pathways are allowed, respectively.[34] Consequently, high Na^+ mobility is expected for pyrophosphates including $Na_{1.56}Fe_{1.22}P_2O_7$. In our previous study, it has been demonstrated that the charge transfer between the ions in the electrolyte and the electrons at the electrode surface is facilitated at elevated temperatures.[24] Overall, an enhanced high rate performance is achieved for $Na_{1.56}Fe_{1.22}P_2O_7$ compared to $Na_2FeP_2O_7$. The charge–discharge curves for the rate capability test are shown in Fig. S2 (Supplementary material).

The long term cycling performance of the $Na_{1.56}Fe_{1.22}P_2O_7$ electrode at a current density of 1 C (118 mA g^{-1}) at 298, 323, and 363 K is shown in Fig. 5. A remarkably stable cycling behavior with negligible capacity decay (<1.5%) over 300 cycles is observed in all the cases. The average coulombic efficiencies over the course of the entire test are 99.9%, 99.8%, and 99.7% at 298 K, 323 K, and 363 K, respectively, indicating the absence of undesirable side reactions. When cycled at a high rate of 20 C (2360 mA g^{-1}) at 363 K, 71% of the initial capacity is retained after 3000 cycles and the coulombic efficiency averages at around 99.95% (Fig. 6). For reference, the charge–discharge curves at 20 C at 363 K are shown in Fig. S3 (Supplementary material). It has been reported that the volume change between the fully desodiated and sodiated $Na_{1.56}Fe_{1.22}P_2O_7$ is 1.9%,[18] which is extremely small compared to other phosphate-based materials including $NaFePO_4$ (17.6%),[35] $Na_3V_2(PO_4)_3$ (8.3%),[36] $Na_4Fe_3(PO_4)_2P_2O_7$ (4%),[37] and $Na_2FeP_2O_7$ (2.6%).[11] The outstanding cyclability is attributed to the negligible volume variation of the rigid pyrophosphate framework owing to its low sensitivity to Na insertion/extraction as well as the use of a chemically stable IL electrolyte (Na[FSA]–[C_3C_1pyrr][FSA]). The present result is reminiscent of the well-known zero-strain $Li_4Ti_5O_{12}$[38]

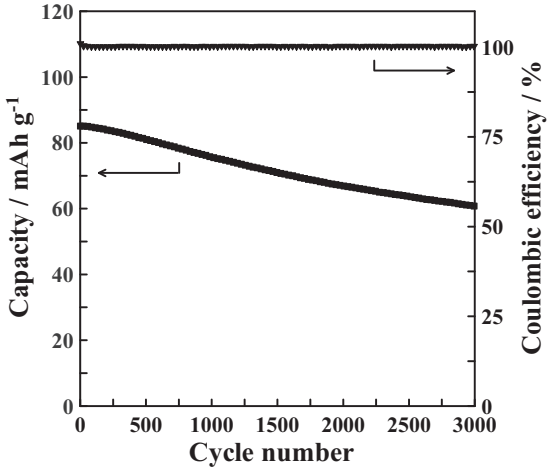

Figure 6. Cycling performance and coulombic efficiency of the $Na_{1.56}Fe_{1.22}P_2O_7$ positive electrode at 363 K. Cut-off voltage: 2.0–4.0 V; current density: 20 C (2360 mA g^{-1}).

electrode for Li secondary batteries, which highlights the importance of using electrode materials exhibiting small volume change in order to achieve high cycle stability.[34] Although the theoretical capacity of $Na_{1.56}Fe_{1.22}P_2O_7$ is lower than the recently reported layered oxides,[7,8] the rate capability and cyclability achieved here recommend this material as a strong candidate as positive electrode for Na secondary batteries.

Conclusions

The electrochemical properties of the end members of $Na_{2-x}Fe_{1+x/2}P_2O_7$ ($Na_2FeP_2O_7$ and $Na_{1.56}Fe_{1.22}P_2O_7$ where $x = 0$ and 0.44, respectively) have been investigated and compared in Na[FSA]–[C_3C_1pyrr][FSA] IL electrolytes over the temperature range of 298–363 K. By altering the Na/Fe stoichiometric ratio, $Na_{1.56}Fe_{1.22}P_2O_7$ exhibits a reversible capacity of 108 mAh g^{-1} at 363 K, which is 15% improved than that of $Na_2FeP_2O_7$ at the same condition. In addition, it also exhibits an enhanced high rate performance and a remarkably stable cyclability. These superior charge–discharge characteristics have been demonstrated for the first time by adopting a thermally and chemically stable IL electrolyte. The positive electrode material is composed of abundantly available elements including Fe, P, and Na, and can be prepared by a scalable solid-state method, which encourages further development of polyanionic compounds through composition design.

Acknowledgments

This study was partly supported by Advanced Low Carbon Technology Research and Development Program (ALCA) of Japan Science and Technology Agency (JST) and Japanese Ministry of Education, Culture, Sports, Science and Technology (MEXT) program "Elements Strategy Initiative to Form Core Research Center".

References

1. V. Palomares, M. Casas-Cabanas, E. Castillo-Martinez, M. H. Han, and T. Rojo, *Energy Environ. Sci.*, **6**, 2312 (2013).
2. M. S. Islam and C. A. J. Fisher, *Chem. Soc. Rev.*, **43**, 185 (2014).
3. P. Serras, V. Palomares, J. Alonso, N. Sharma, J. M. L. del Amo, P. Kubiak, M. L. Fdez-Gubieda, and T. Rojo, *Chem. Mater.*, **25**, 4917 (2013).
4. R. Berthelot, D. Carlier, and C. Delmas, *Nat. Mater.*, **10**, 74 (2011).
5. P. Vassilaras, X. H. Ma, X. Li, and G. Ceder, *J. Electrochem. Soc.*, **160**, A207 (2013).
6. S. Komaba, N. Yabuuchi, T. Nakayama, A. Ogata, T. Ishikawa, and I. Nakai, *Inorg. Chem.*, **51**, 6211 (2012).
7. N. Yabuuchi, M. Kajiyama, J. Iwatate, H. Nishikawa, S. Hitomi, R. Okuyama, R. Usui, Y. Yamada, and S. Komaba, *Nat. Mater.*, **11**, 512 (2012).
8. J. Billaud, G. Singh, A. R. Armstrong, E. Gonzalo, V. Roddatis, M. Armand, T. Rojo, and P. G. Bruce, *Energy Environ. Sci.*, **7**, 1387 (2014).

9. K. Saravanan, C. W. Mason, A. Rudola, K. H. Wong, and P. Balaya, *Adv. Energy Mater.*, **3**, 444 (2013).
10. P. Barpanda, T. Ye, S. Nishimura, S. C. Chung, Y. Yamada, M. Okubo, H. S. Zhou, and A. Yamada, *Electrochem. Commun.*, **24**, 116 (2012).
11. P. Barpanda, G. D. Liu, C. D. Ling, M. Tamaru, M. Avdeev, S. C. Chung, Y. Yamada, and A. Yamada, *Chem. Mater.*, **25**, 3480 (2013).
12. H. Kim, R. A. Shakoor, C. Park, S. Y. Lim, J. S. Kim, Y. N. Jo, W. Cho, K. Miyasaka, R. Kahraman, Y. Jung, and J. W. Choi, *Adv. Funct. Mater.*, **23**, 1147 (2013).
13. C. S. Park, H. Kim, R. A. Shakoor, E. Yang, S. Y. Lim, R. Kahraman, Y. Jung, and J. W. Choi, *J. Am. Chem. Soc.*, **135**, 2787 (2013).
14. J. M. Clark, P. Barpanda, A. Yamada, and M. S. Islam, *J. Mater. Chem. A*, **2**, 11807 (2014).
15. P. Barpanda, T. Ye, M. Avdeev, S. C. Chung, and A. Yamada, *J. Mater. Chem. A*, **1**, 4194 (2013).
16. P. Barpanda, J. C. Lu, T. Ye, M. Kajiyama, S. C. Chung, N. Yabuuchi, S. Komaba, and A. Yamada, *RSC Adv.*, **3**, 3857 (2013).
17. T. Honma, N. Ito, T. Togashi, A. Sato, and T. Komatsu, *J. Power Sources*, **227**, 31 (2013).
18. K. H. Ha, S. H. Woo, D. Mok, N. S. Choi, Y. Park, S. M. Oh, Y. Kim, J. Kim, J. Lee, L. F. Nazar, and K. T. Lee, *Adv. Energy Mater.*, **3**, 770 (2013).
19. M. Armand, F. Endres, D. R. MacFarlane, H. Ohno, and B. Scrosati, *Nat. Mater.*, **8**, 621 (2009).
20. D. R. MacFarlane, N. Tachikawa, M. Forsyth, J. M. Pringle, P. C. Howlett, G. D. Elliott, J. H. Davis, M. Watanabe, P. Simon, and C. A. Angell, *Energy Environ. Sci.*, **7**, 232 (2014).
21. N. Wongittharom, T. C. Lee, I. M. Hung, S. W. Lee, Y. C. Wang, and J. K. Chang, *J. Mater. Chem. A*, **2**, 3613 (2014).
22. N. Wongittharom, T. C. Lee, C. H. Wang, Y. C. Wang, and J. K. Chang, *J. Mater. Chem. A*, **2**, 5655 (2014).
23. D. Monti, E. Jonsson, M. R. Palacin, and P. Johansson, *J. Power Sources*, **245**, 630 (2014).
24. C. Y. Chen, K. Matsumoto, T. Nohira, C. S. Ding, T. Yamamoto, and R. Hagiwara, *Electrochim. Acta*, **133**, 583 (2014).
25. C. Y. Chen, K. Matsumoto, T. Nohira, R. Hagiwara, Y. Orikasa, and Y. Uchimoto, *J. Power Sources*, **246**, 783 (2014).
26. F. Izumi and K. Momma, *Solid State Phenom.*, **130**, 15 (2007).
27. K. Momma and F. Izumi, *J. Appl. Crystallogr.*, **44**, 1272 (2011).
28. C. S. Ding, T. Nohira, K. Kuroda, R. Hagiwara, A. Fukunaga, S. Sakai, K. Nitta, and S. Inazawa, *J. Power Sources*, **238**, 296 (2013).
29. J. Angenault, J. C. Couturier, M. Quarton, and F. Robert, *Eur. J. Solid State Inorg. Chem.*, **32**, 335 (1995).
30. G. Kobayashi, S. Nishimura, M. S. Park, R. Kanno, M. Yashima, T. Ida, and A. Yamada, *Adv. Funct. Mater.*, **19**, 395 (2009).
31. J. F. Martin, A. Yamada, G. Kobayashi, S. Nishimura, R. Kanno, D. Guyomard, and N. Dupre, *Electrochem. Solid-State Lett.*, **11**, A12 (2008).
32. S. W. Kim, D. H. Seo, X. H. Ma, G. Ceder, and K. Kang, *Adv. Energy Mater.*, **2**, 710 (2012).
33. J. M. Clark, P. Barpanda, A. Yamada, and M. S. Islam, *J. Mater. Chem. A*, **2**, 11807 (2014).
34. R. Tripathi, S. M. Wood, M. S. Islam, and L. F. Nazar, *Energy Environ. Sci.*, **6**, 2257 (2013).
35. M. Casas-Cabanas, V. V. Roddatis, D. Saurel, P. Kubiak, J. Carretero-Gonzalez, V. Palomares, P. Serras, and T. Rojo, *J. Mater. Chem.*, **22**, 17421 (2012).
36. Z. L. Jian, W. Z. Han, X. Lu, H. X. Yang, Y. S. Hu, J. Zhou, Z. B. Zhou, J. Q. Li, W. Chen, D. F. Chen, and L. Q. Chen, *Adv. Energy Mater.*, **3**, 156 (2013).
37. H. Kim, I. Park, D. H. Seo, S. Lee, S. W. Kim, W. J. Kwon, Y. U. Park, C. S. Kim, S. Jeon, and K. Kang, *J. Am. Chem. Soc.*, **134**, 10369 (2012).
38. T. Ohzuku, A. Ueda, and N. Yamamoto, *J. Electrochem. Soc.*, **142**, 1431 (1995).